Granular Matter
DOI 10.1007/s10035-014-0515-3

ORIGINAL PAPER

Distinct simulation of earth pressure against a rigid retaining wall considering inter-particle rolling resistance in sandy backfill

Mingjing Jiang · Jie He · Jianfeng Wang · Fang Liu · Wangcheng Zhang

Received: 11 May 2013

Abstract The focus of this paper is to analyze earth pressure against a rigid retaining wall under various wall movement modes with a contact model considering inter-particle rolling resistance implemented into the distinct element method (DEM). Firstly, a contact model considering rolling resistance in particles was generally explained and implemented into the DEM. The parameters of the contact model are determined from DEM simulation of biaxial tests on a sandy specimen. Then, the influence of inter-particle rolling resistance in the backfill is discussed by comparing the active and passive earth pressure against a rigid wall subjected to a translational displacement with and without inter-particle rolling resistance in the material. Third, the DEM model considering the rolling resistance is used to investigate active and passive earth pressures while the rigid wall moves in a more general manner such as rotation or translation. The influence of rolling resistance on the earth pressures is examined from the microscopic particle scale (e.g., shear strain field) as well as the macroscopic scale (e.g., the magnitude and action point of resultant earth pressures). Finally, the effect of the initial density and the particle size of the backfill are discussed. The results show that when rolling resistance in the particles is taken into account in the DEM simulation, the simulation results are more appropriate and are in line with practical situation. Hence, particles rolling resistance should be taken into account to get more realistic results in DEM analyses.

Keywords Distinct element method · Earth pressure · Displacement mode · Rolling resistance

M. Jiang (✉) · J. He · F. Liu · W. Zhang
Department of Geotechnical Engineering, College of Civil Engineering, Tongji University, Shanghai 200092, China
e-mail: mingjing.jiang@mail.tongji.edu.cn

M. Jiang · J. He · F. Liu · W. Zhang
State Key Laboratory for Disaster Reduction in Civil Engineering, Tongji University, Shanghai 200092, China

J. Wang
Department of Civil and Architectural Engineering, City University of Hong Kong, Hong Kong, China

1 Introduction

Estimating the earth pressure against retaining structures is an antique and classical problem in soil mechanics, which has been studied for over 200 years since the pioneering works by Coulomb [1] and Rankine [2]. Besides theoretical approach [3–7] and experimental approach [8–18], numerical simulation is an effective alternative for investigating the earth pressure distribution with higher flexibility in coping with a variety of boundary conditions and constitutive behaviors of backfills. Some researchers adopted the finite element method (FEM) to study the earth pressure problems [19–24]. The earth pressure problem is accompanied with strain localization and failure. The deformation within the granular materials tends to localize along concentrated bands, named shear bands, resulting from non-uniform stress state or trivial defects within an element. The modeling of this localization phenomenon is important, since many engineering structure failure is indeed characterized by the formation and propagation of shear bands [25–30]. And this brings about one of the bottlenecks in finite element simulation that originated from the continuum mechanics [31]. The FEM based on some advanced constitutive laws can partially model strain localization. For example, in the theory of micro-polar continuum (or Cosserat continuum), two linked levels of deformation are considered: micro-rotation at the particle level and macro-deformation at the structural level [32–35]. The rotational degrees of freedom of material

Published online: 21 June 2014

particles are introduced to surpass the limitation of the conventional continuum in modeling shear localization phenomenon [32]. However, the shear band configuration in granular materials was influenced by many factors such as pressure level, void ratio, mean grain diameter, grain roughness, grain hardness and the stiffness of the surrounding structure in contact with a granular body [33], all of which should be independent of the mesh configuration. In contrast, the conventional finite element results do not depend on the size and orientation of the mesh in strain localization analyses if they equipped with a characteristic length of micro-structure as well as the mesh size is small enough, while the inclinations of shear band predicted by finite element method (FEM) are obviously smaller than the real value even if the constitutive model is equipped with a characteristic length of micro-structure (e.g., micro-polar, second-gradient, non-local models). Within a micro-polar continuum, a characteristic length of micro-structure corresponds to a mean grain diameter. However, there is no universal agreement on the characteristic length of micro-structure in the constitutive models yet [36]. Although there exist already some realistic two-scale numerical approaches to study the behavior of granular materials [37,38] and the two-scale distinct element method (DEM)–FEM appears a good way to depict the behavior of granular material, there is a gap between micro and macro mechanics on granular material. For example, no agreement has been made on the definition linking microscopic contact behavior between particles and macroscopic strain tensor for such granular material. It is known that if the macroscopic strain tensor is linked with the translational motion of grain centers, as done in geo-experiment, there needs to introduce a variable named 'the average pure rotation rate' or APR in short [39], which is proposed to describe particle rotation of REV and which is found very large within shear band. In addition, it is known that the rolling resistance at particle contacts comes microscopically from grain roughness or shape effect [39,40]. Similar to the interpretation of the internal length in Chang's couple-stress continuum for bonded granulates [41], it appears that a characteristic length of a Cosserat continuum should be linked to microscopic parameters controlling the rolling resistance instead of others. However, from a theoretical point of view, micro and macro (defined in a consistent framework) have to strictly converge when the number of grains is tending to infinity. Besides, an assembly of granular material may demonstrate complex mechanical behavior. For example, during a whole process of landslide, it behaves as a solid before the landslide starts, then as a liquid named granular flow during landslide, and finally becomes a solid again after it has moved a run-out distance and stops moving. This phenomenon is quite difficult to be simulated using a macroscopic constitutive model. Even in the quasi-static framework, an assembly of granular material will show other complex mechanical behavior, such as grain crushing, under loading, which demands proper macroscopic constitutive models in future [42]. Finally, continuum-based approaches are frequently phenomenological in nature, implying that many of their model parameters may lack clear physical meaning and well-defined calculation procedure.

In contrast, the DEM based on discrete mechanics theory, has obvious advantages to solve large deformation and failure problems [43–46]. Compared to FEM numerical simulation method, the DEM advantage in dealing with the earth pressure problem is that only some basic microscopic parameters of the sand particles (such as the contact stiffness and friction coefficient, etc.) are needed for the simulation, and the soil constitutive relationship can be born automatically, thus avoiding selecting the constitutive relation and its parameters. The DEM results also tend to be more accurate. In addition, when dealing with the soil-wall interface, the friction coefficient between the wall and sand particles can be given. This is very simple and the meaning is clear [47]. More importantly, DEM can provide insights into the micro-mechanics of the soil under the influence of some specific particle-scale mechanical properties, such as the rolling resistance being studied in this paper to represent the effect of particle shape.

DEM can capture the main characteristics of clean or cemented granular materials, which has been attracting increasing research interests in geo-mechanics community since firstly proposed [43]. The DEM characterizes soil properties at the particle level with simple inter-particle contact laws, which have been widely used to investigate soil behaviors [30,47–49]. Although as a result of the limitation of the calculation capability of current computers, it is still difficult to simulate large geotechnical problems by DEM, especially in the case that a true-scale system is to be reproduced with an extremely large number of particles. Although, it is not possible to completely eliminate the size/scale effect of a DEM model which contains insufficient number of particles or ratio of specimen to mean grain size as compared to the actual laboratory or field-scale model. However, the model behavior allows the understanding of the physical principles governing the macroscopic soil behavior as long as a characteristic mode of strain localization (e.g., a uniform global failure mode or a progressive failure mode) can be captured [50]. The shear strength of a granular specimen displaying a uniform global failure mode represents its true full strength, while that corresponding to a progressive failure mode represents a nominal, less-than-full strength. Which case should be used in the interpretation of a full-scale field behavior depends on the exact strain localization mode occurring in the field, which is a complex function of the soil condition, boundary condition and loading condition. The size/scale effect, provided that there is an enough ratio of specimen to mean grain size in the DEM model, will then not be a big concern. The pressure level affects also the DEM

results for small granular specimens. It is a basic knowledge in Soil Mechanics that initially dense soils may demonstrate 'strain-hardening' relationship between deviator stress and strain together with shear-contraction under high confining pressures, although they show 'strain-softening' relationship together with shear-dilatancy under low confining pressures. Such a pressure-dependent behavior can be naturally captured by DEM material in element tests. It can also be well reflected in DEM analyses of boundary-value problems. In order to reproduce the stress state in the actual field engineering problems or laboratory-scale physical model tests (e.g., centrifuge test), a large size of the specimen with the original gravity can be used if one has supercomputers or a small size of the specimen with an amplified gravity (ng) can be employed if one has PCs. Therefore, some researchers have used this method to analyze boundary-value problems [51–54] including earth pressure-related problems [55–58].

Particle rotation has been found to be significant in affecting the behavior of granular materials. Inter-particle rolling, as a micro-scale deformation mechanism, affects the peak strength of granular materials, and leads to extensive dilatancy of granular media [59–63]. Particle rotation has also been regarded as an important factor in elastic micromechanical models [64–66]. Thus to study the earth pressure against the rigid wall, considering inter-particle rolling resistance is very necessary.

Several contact models considering particle rolling resistance have been proposed [61,64,67,68], among which the model proposed by Iwashita and Oda [61] is well known. However this model needs several parameters to define rolling resistance, which needs to be determined through trial and error. In view of this limitation, Jiang et al. [69] proposed another rolling resistance contact model (Jiang's model for short) for granular materials, which consists of a geometrically derived kinematical model, physically based mechanical contact models and locally equilibrated equations governing the motion of the rigid particles. Only one parameter is needed to quantify the rolling resistance in Jiang's model. So, in this study, this new rolling resistance contact model will be used to analyze the earth pressure problem.

The paper aims to analyze the earth pressure against a rigid wall subjected to various displacement modes with the contact model considering inter-particle rolling resistance. For this aim, Jiang's model is implemented in a DEM software [46] and the parameters of the contact model are first determined from a DEM simulation of biaxial tests on a sandy specimen. The influence of inter-particle rolling resistance in the backfill is then discussed by comparing the active and passive earth pressure against a rigid wall subjected to a translational displacement with and without inter-particle rolling resistance in the material. Next, the DEM considering the rolling resistance is used to investigate active and passive earth pressures while the rigid wall moves in a more general manner such as rotation or translation. The influence of rolling resistance on the earth pressures is examined from the microscopic particle scale (e.g., shear strain field) as well as the macroscopic scale (e.g., the magnitude and action point of resultant earth pressures). Finally, several other factors such as the initial density and the mean grain size are discussed in detail.

2 A contact model for granular materials considering inter-particle rolling resistance

Jiang et al. [69] proposed a contact model for considering the inter-particle rolling resistance in granular materials such as soils. The standard DEM assumption that grains are in contact at discrete points was replaced here by the assumption that grains are in contact over a width. Assuming that normal/tangential basic elements continuously distributed along the grain contact width, Jiang et al. [69] established a rolling contact model in addition to normal/tangential contact models, and also related the governing equations to local equilibrium. The model only introduces one parameter, i.e. rolling resistance coefficient δ, to reflect the actual situation between particles. Because only one parameter δ is needed in comparison to the standard DEM, the model has solved the drawback of having a lot of parameters which are difficult to determine in a typical discrete element in [61].

Figure 1 demonstrates schematic illustration of the contact model proposed for grains and its mechanical response. The complete mechanical contact model is composed of normal, tangential and rolling contact components, in which a normal contact model is to resist normal force, a tangential contact model to resist shear force and a rolling contact model to resist rolling. In Fig. 1b, a normal contact model does not bear the tension, and the model only resists normal pressure which is proportional to the amount of particle overlap, namely,

$$F_n = k_n \times u_n \tag{1}$$

where k_n is the normal contact stiffness (in N/m in a two-dimensional system), and u_n is the overlap amount of inter-particles.

Figure 1c shows that the tangential force is proportional to the tangential displacement and is calculated by incremental method, which can be seen in Eq. (2). The tangential force increases linearly within a certain range of particles relative sliding displacements, and then maintains a constant value when tangential force reaches to maximum value which is determined by friction coefficient multiplied by the normal contact force.

$$F_s = k_s \times u_s \tag{2}$$

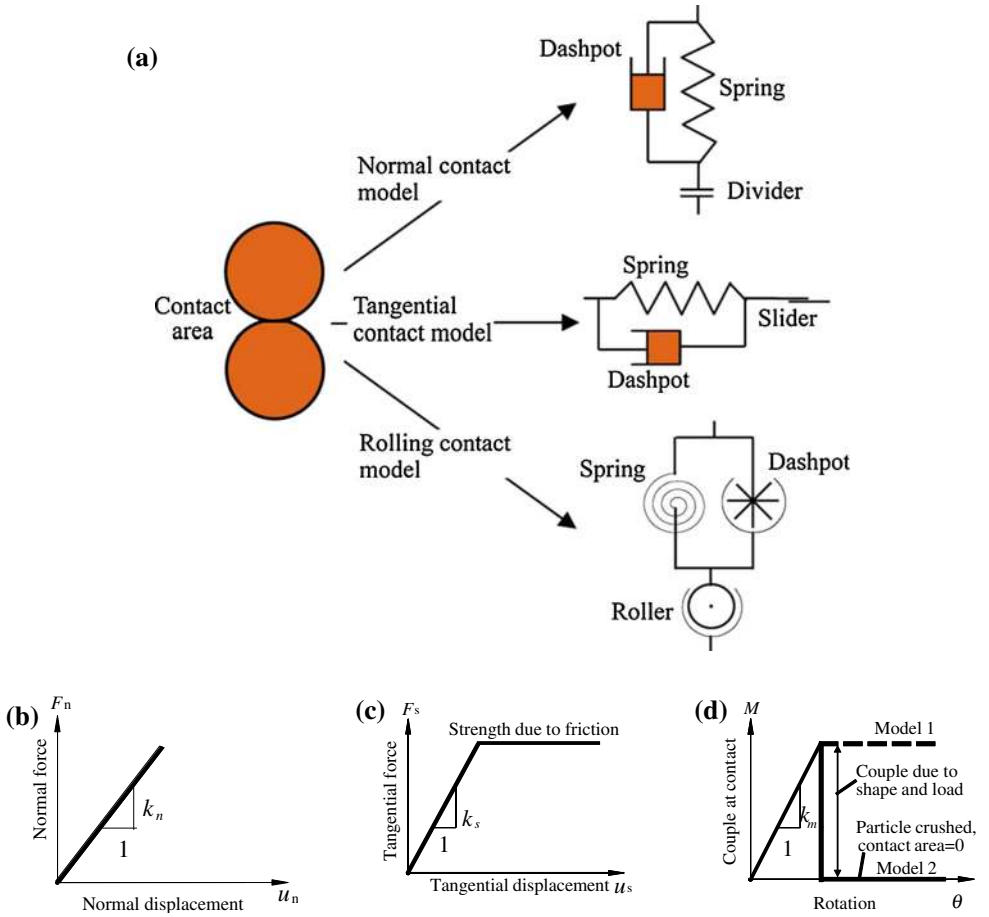

Fig. 1 Schematic illustration of the contact model proposed for grains and its mechanical response: **a** a contact model with rolling resistance; **b** normal direction; **c** tangential direction; **d** rolling direction

where k_s is the tangential contact stiffness, and u_s is the tangential relative displacements between the particles.

The rolling contact model is characterized by the stiffness k_m; when the plastic rolling occurs, the rolling resistance at the contact is maintained at a value defined by Mohr–Coulomb type criterion in Model 1 or abruptly reduces to zero in Model 2 in Fig. 1d. This paper chooses Model 1 in calculation. Note that non-classical medium, such as Cosserat mechanics, is assumed here, and therefore the presence of the couple stresses gives rise to non-symmetry of the stress tensor. However, there is a gap between micro-mechanics and macro-mechanics on granular material. The couple between the particles is calculated by incremental method and relates to these factors, rolling resistance coefficient, particle contact normal force, average particle radius and relative rotation velocity. It is calculated as follows:

$$M = \begin{cases} k_m \times \theta & \theta \le \theta^r \\ M^p & \theta \ge \theta^r \end{cases} \tag{3}$$

where M is the couple at contact; M^p is peak couple at contact, which is numerically equal to k_m multiply by θ^r; θ^r is the critical relative rotation angle according to Eq. (4); k_m is the rolling contact stiffness, which is determined by Eq. (5).

$$\theta^r = \frac{2 \times F_n}{k_n \times r \times \delta} \tag{4}$$

where δ is the rolling resistance coefficient.

$$k_m = \frac{k_n \times r^2 \times \delta^2}{12} \tag{5}$$

where r is the average radius of the contact particles, namely:

$$r = \frac{2r_1 r_2}{r_1 + r_2} \tag{6}$$

where r_1 and r_2 are the radius of two contact particles respectively.

Couple damping coefficient doesn't need to additionally specify and can be calculated as follows through the normal damping coefficient:

$$\mu_m = \mu_n \times \frac{r^2 \times \delta^2}{12} \tag{7}$$

where μ_m is couple damping coefficient; μ_n is normal damping coefficient. Note that Eqs. (4), (5) and (7) are based on solid mechanics, and their validity has been numerically checked by Jiang et al. [69]. The detailed formulation can be read from [61]. The salient features of the formulation are: (1) it consists of a geometrically derived kinematical model, physically based mechanical contact models and locally equilibrated equations governing the motion of the rigid particles; (2) Only one additional parameter δ needs to be introduced in the model when compared with the standard DEM.

It is known that rolling resistance (couple) does not affect the translational motions of grains but does affect the angular motion of grains. Hence, the couple at each direct contact must be summed up in affecting the angular motion of a grain. For disc j with radius r_j, the contact forces $F_n^{(q)}$, $F_s^{(q)}$ and couple $M^{(q)}$ are summed over p neighbors, which then govern the motion of the disc in both X and Y directions and the rotation about the center of mass shown in Eq. (8).

$$\ddot{x}_i^j = \frac{1}{m^j}\sum_{q=1}^{p} F_i^{(q)}, \qquad \ddot{\theta}^j = \frac{1}{I^j}\left(\sum_{q=1}^{p} r_j F_s^{(q)} + \sum_{q=1}^{p} M^{(q)}\right) \tag{8}$$

where $F_i^{(q)}$ is x_i component of the resultant force at contact q and $i = 1, 2$, representing X and Y directions, respectively.

3 DEM model of retaining wall

The DEM model of a retaining wall was made to facilitate a direct comparison with the experimental results of Fang et al. [16], Fang and Ishibashi [17] and Fang et al. [18]. A series of model tests was conducted under plane-strain conditions to investigate the active and passive earth pressure in response to different wall displacement modes using two rigid model walls: one was 0.5 m high [16,18] and the other was 1.0 m high [17]. The air-dried Ottawa silica sand was used in the model tests with the relative densities ranging from 19.2 to 80 %, indicating a variety of density conditions. Table 1 lists a few key model parameters used in their tests.

To compare DEM results directly with the experimental test of Fang and Ishibashi [17], the plane strain discrete calculations were performed with a gravitational field of $5g$. Figure 2 presents the DEM model of the retaining wall with the sandy backfill. The model size of the ground is 625 mm wide and 250 mm high. Under the action of $5g$ gravity field, the model is 3.125 m wide and 1.25 m high, filled with a poly-dispersed, well-compacted granular assembly which is composed of rigid 103,132 discs with the diameters uniformly ranging between 0.78 and 1.94 mm giving a mean diameter d_{50} of 1.36 mm. The multi-layer under-compaction technique proposed in [70] was used to generate the homogeneous samples with different target values of the void ratio, i.e., $e = 0.20, 0.22, 0.25, 0.33$, representing a variety of packing conditions ranging from very dense to very

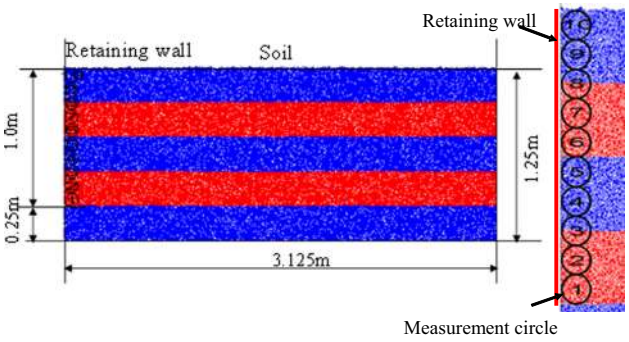

Fig. 2 DEM model of the retaining wall with the layout of measurement circles

Table 1 Summary of model parameters used in the model tests [16–18]

Test no.	Displacement mode	Dr (%)	Wall height (m)	Peak internal friction angle	Residual internal friction angle	References
1	Passive T	38	0.5	33.0°	31.5°	Fang et al. [16]
2	Passive T	63	0.5	38.3°	31.5°	Fang et al. [16]
3	Passive T	80	0.5	42.1°	31.5°	Fang et al. [16]
4	Active T	24.8	1.0	34.0°	–	Fang and Ishibashi [17]
5	Active RT	30.1	1.0	34.9°	–	Fang and Ishibashi [17]
6	Active RB	21.4	1.0	33.4°	–	Fang and Ishibashi [17]
7	Passive T	19.2	0.5	30.9°	–	Fang et al. [18]
8	Passive RT	19.2	0.5	30.9°	–	Fang et al. [18]
9	Passive RB	19.2	0.5	30.9°	–	Fang et al. [18]

Table 2 Model parameters used in the DEM simulations

Parameters	Value
Total number in sample	103,132
Particle density (kg/m^3)	2,600
Initial void ratio	0.20, 0.22, 0.25, 0.33
Inter-particle normal contact stiffness (N/m)	7.5×10^7
Inter-particle tangential contact stiffness (N/m)	5.0×10^7
Interparticle coefficient of friction	0.7
Wall-particle normal stiffness (N/m)	7.5×10^7
Wall-particle tangential stiffness (N/m)	5.0×10^7
Coefficient of wall friction	0.5
Rolling resistance	0, 1.0

loose. Each initial void ratio of the samples was achieved by generating and compacting five equal sub-layers of granular materials, with the planar void ratio of each new sub-layer being slightly smaller than that of the previous accumulated sub-layers. The initial void ratio $e = 0.25$, representing a medium-dense material with slight strain softening and volumetric dilatancy, is used as the basic case to be analyzed in Sects. 4–6, while the results obtained from other void ratios will be discussed in detail in Sect. 7. The DEM parameters of the granular material used in this study are provided in Table 2. These parameters were obtained from the model calibration on a series of DEM simulations of the biaxial compression tests, which ultimately produced realistic macroscopic mechanical properties (e.g., the internal friction angle in this study) comparable to the experimental data.

As shown in Fig. 2, the mobile retaining wall is made of the upper 1 m-high section of the left boundary, with the lower 0.25 m-high section being fixed. In this study, three displacement modes of the retaining wall, namely, translation (T mode), rotation about the bottom of the wall (RB mode) and rotation about the top of the wall (RT mode) are simulated and the lateral earth pressure induced by these three displacement modes under the active and passive states are investigated. In order to measure the stress state of filled soil behind the retaining wall under different displacement modes, ten measurement circles with the equal radius of 0.05 m were placed behind the retaining wall (Fig. 2). These measurement circles, each containing about 200 particles, can move simultaneously with the retaining wall subjected to various displacement modes. The average stress tensor $\bar{\sigma}_{ij}$ was calculated in each pre-defined measurement circle that covers a volume of V by the following equation:

$$\bar{\sigma}_{ij} = \frac{1}{V} \sum_{N_p} \bar{\sigma}_{ij}^{(P)} V^{(P)} \tag{9}$$

where N_p is the number of particles within the volume V; and $\bar{\sigma}_{ij}^{(P)}$ is the average stress tensor in particle (P) with a volume of $V^{(P)}$, and it can be computed by:

$$\bar{\sigma}_{ij}^{(p)} = -\frac{1}{V^{(p)}} \sum_{N_c} \left| x_i^{(c)} - x_i^{(p)} \right| n_i^{(c,p)} F_j^{(c)} \tag{10}$$

where N_c is the number of contact; $x_i^{(c)}$, $F_j^{(c)}$ are the location and force, respectively, acting at contact (c); $x_i^{(p)}$ is the location of the particle centroid; $n_i^{(c,p)}$ is the unit-normal vector directed from the particle centroid to the contact location, and is a function of both the contact and the particle.

The schematic diagrams illustrating the three displacement modes under the active and passive states are shown in Figs. 3 and 4, respectively. The velocities of the translating retaining wall are 1.3×10^{-4} and 6.5×10^{-4} m/s in active T mode and passive T mode, respectively; and the rotation velocity of the retaining wall is 6.5×10^{-4} rad/s. These values were chosen by justifying the velocities until the quasi-static conditions were satisfied. Note that although real granular materials demonstrate rate-dependent behavior in laboratory [42], the retaining wall velocities can be neither too large nor too small in the DEM simulations. If the wall moves too fast, the particles behind the wall cannot synchronously move together with the wall especially in the active modes. If the wall moves too slowly, the simulation will become unaffordable due to high computational cost.

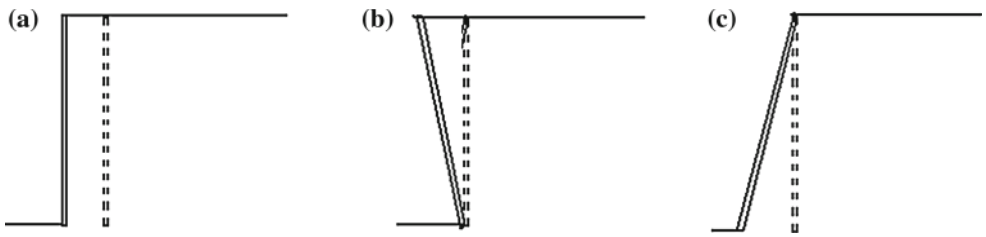

Fig. 3 Three types of active wall movement: **a** T mode; **b** RB mode; **c** RT mode

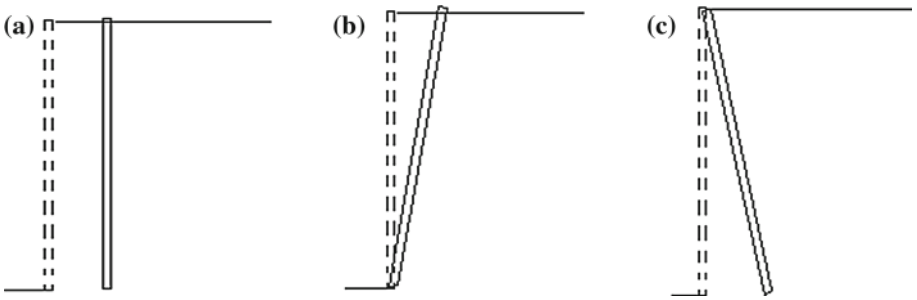

Fig. 4 Three types of passive wall movements: **a** T mode; **b** RB mode; **c** RT mode

4 Influence of inter-particle rolling resistance

Figure 5 presents the effect of the rolling resistance coefficient on the peak and residual internal friction angle obtained from biaxial compression simulations on a sample with $e = 0.25$. It is obvious that the peak and residual friction angles increase with the increasing of rolling resistance coefficient. A realistic value of the internal friction angle of soils can be produced by using the rolling resistance contact model with a properly selected value of δ. In the current study, the rolling resistance coefficient should take such a value that the residual internal friction angle is equal to 30°, if the DEM results will be completely compared to experimental data obtained from tests on real sands. However, we did not aim to simulate a realistic granular material completely (e.g., Ottawa silica sand) with a 2D DEM. The detailed explanation will be illustrated in Sect. 7. Instead, we ensure that the rolling resistance coefficient chosen should fall itself into a reasonable range and renders a peak internal friction angle equal to 30°. Hence, the rolling resistance coefficient takes a value of 1.0, which yields the peak friction angle of 29.3° and the residual angle of 22.6°.

In the following, the influence of inter-particle rolling resistance in the granular backfill is demonstrated by comparing the active and passive earth pressures under the T mode computed with ($\delta = 1.0$) and without ($\delta = 0.0$) the inter-particle rolling resistance.

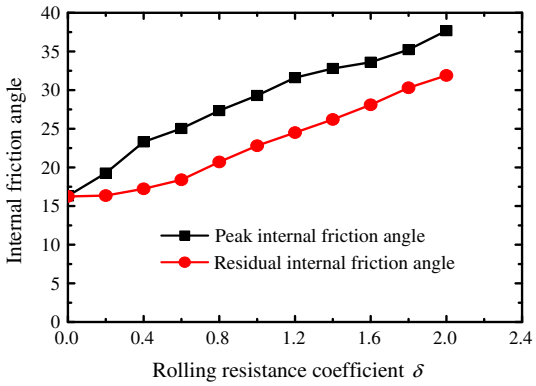

Fig. 5 Relationship between the angle of internal friction and rolling resistance coefficient δ

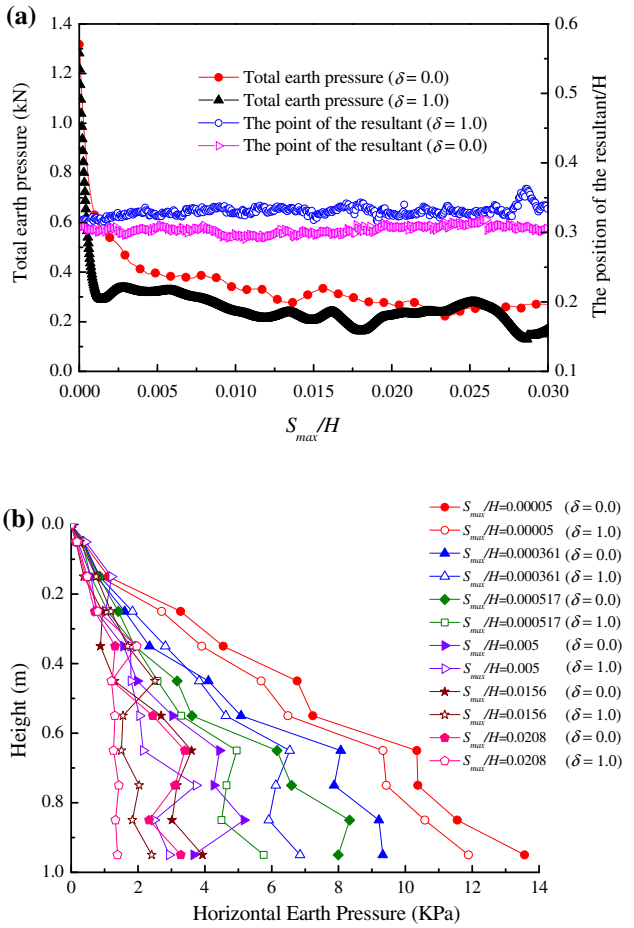

Fig. 6 Influence of inter-particle rolling resistance on active earth pressure in T mode: **a** total earth pressure and its point of the resultant in the two case of $\delta = 0.0$ and $\delta = 1.0$; **b** distribution of earth pressures along the depth of the wall

Figure 6a compares the active total earth pressure and its point of the resultant in the two cases of $\delta = 0.0$ and $\delta = 1.0$. Figure 6a shows that when the wall moves away from the soil mass, the total earth pressures of both cases firstly decrease then reach a relatively stable value. The total active earth pressure profile of $\delta = 1.0$ is apparently lower than that of $\delta = 0.0$. The point of the resultant in the case of $\delta = 0.0$ is located at the 0.3H, which is slightly lower than that of $\delta = 1.0$. Figure 6b provides the distributions of earth

pressure along the height of the wall with different amounts of wall movement (S_{max}/H), in which S_{max} represents the maximum displacement of the rigid retaining wall and H is the height of the wall. It is found that the earth pressure distribution maintains a roughly linear profile and decreases with the increasing wall movement; but at any instance of wall movement, the profile of $\delta = 1.0$ is apparently lower than that of $\delta = 0.0$. This result indicates that given the same amount of lateral strain (i.e., in the sense of biaxial extension with the constant vertical major principal stress), the granular material with inter-particle rolling resistance will mobilize a higher deviator stress.

A similar comparison of the earth pressures under the passive state is presented in Fig. 7. It is clear that the effect of inter-particle rolling resistance is much more pronounced now, reflected in the considerably higher total passive earth pressure profile (Fig. 7a) and the earth pressure distribution profiles of the case of $\delta = 1.0$ (Fig. 7b). This enhanced effect of rolling resistance stems from the much higher deviator stress mobilized in the biaxial compression deformation (with the constant vertical minor principal stress).

Based on the above results, the influence of inter-particle rolling resistance on the lateral earth pressures mobilized in the T mode is obvious. In the following sections, we shall present the simulation results with $\delta = 1.0$ for all the three displacement modes and the associated micromechanical deformation mechanisms.

5 Active earth pressures under different displacement modes

Figure 8 presents the active total earth pressure against the retaining wall and its point of the resultant with the chang-

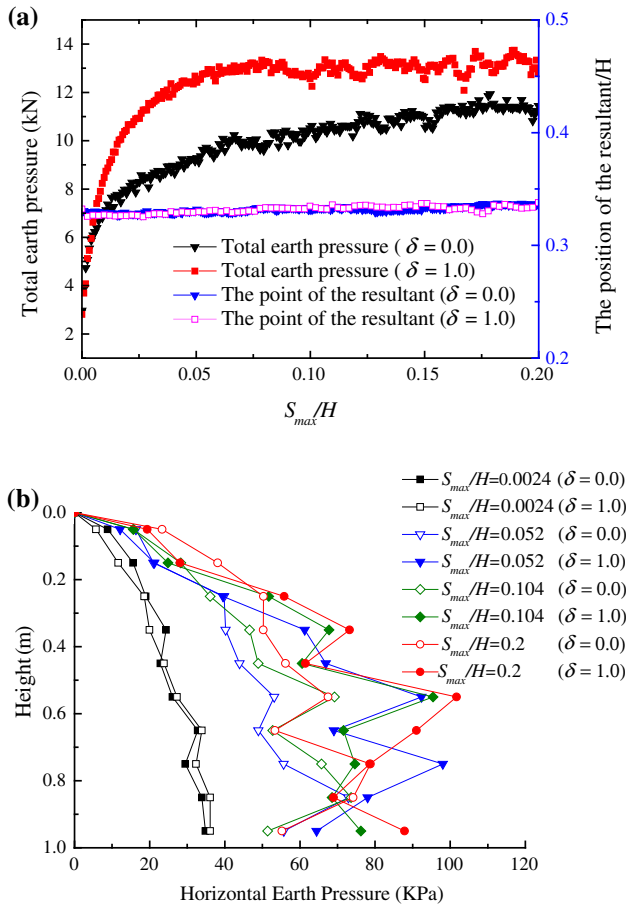

Fig. 7 Influence of inter-particle rolling resistance on passive earth pressure in T mode: **a** total earth pressure and its point of the resultant in the two case of $\delta = 0.0$ and $\delta = 1.0$; **b** distribution of earth pressure along the depth of the wall

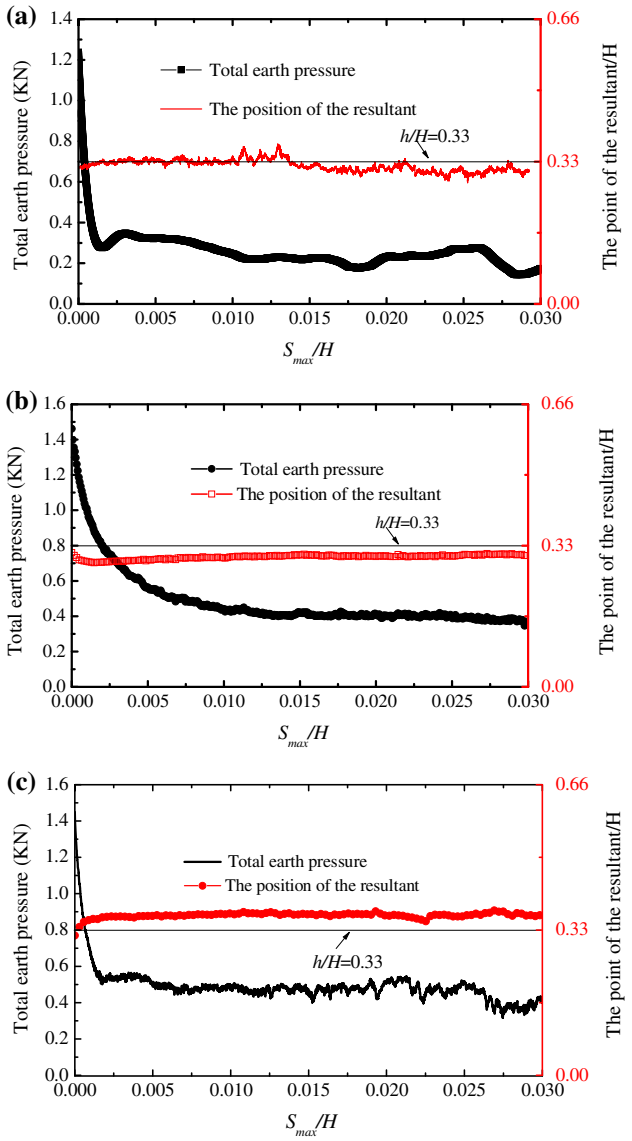

Fig. 8 Total earth pressure against the retaining wall and its point of the resultant with changing displacement in the three modes at active state: **a** T mode; **b** RB mode; **c** RT mode

ing displacement in the three modes. Figure 8 shows that the overall profiles of the total earth pressure are similar for all the cases, with an initial rapid reduction of the earth pressure with the increasing wall displacement followed by a relatively stable regime extending to large displacements. However, the minimum earth pressure achieved in the T mode is obviously less than those in the RB and RT modes. This is attributed to the development of a more extensive strain localization zone within the granular backfill and the associated higher mobilized shear strength in the T mode. More supporting evidence of this statement will be shown below. It is also noted that the minimum earth pressure is achieved at a much larger displacement in the RB mode than in the other two modes. This may be caused by the non-linear behavior of the granular material and different stress states in different displacement modes. Furthermore, the location of the resultant is found to vary in the three cases, with the values of h/H being equal, slightly below and slightly above 0.33 in T mode, RB mode and RT mode, respectively. This observation fully agrees with the expectation since nonlinear profiles of earth pressure distribution will be generated in the two rotation modes, as will be shown below.

Figure 9 presents the normalized resultant active earth pressure coefficient K_h obtained from the DEM simulation, where K_h is defined as the ratio of the normal component of the total thrust to $\gamma H^2/2$. The horizontal earth pressure distributions in the three displacement modes are shown in Figs. 10, 11, and 12, in which the theoretical asymptote according to Coulomb's theory with the related value of the friction angle was added to facilitate a comparison to the analytical results. The values of K_h obtained from the simulations are reasonable in terms of the order of magnitudes compared with the theoretical value according to Coulomb's solution (i.e., $K_\mathrm{h} = 0.304$). The profiles of the earth pressure distribution are roughly linear, biased towards the top of the wall and biased towards the bottom of the wall in T mode, RB mode and RT mode, respectively.

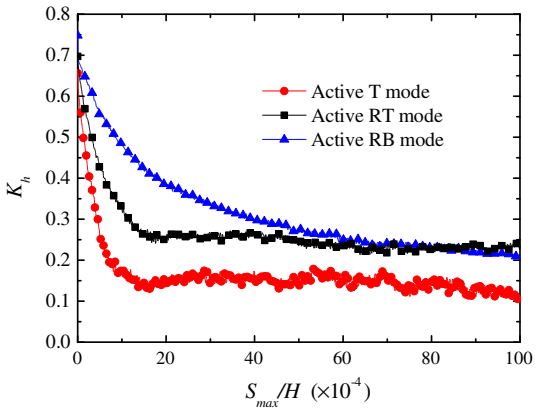

Fig. 9 The normalized resultant active earth pressure coefficient K_h with changing displacement in the three modes at active state obtained from the DEM simulation

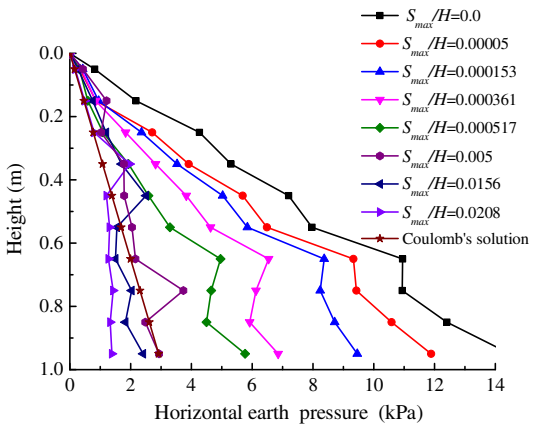

Fig. 10 Distribution of Horizontal Earth Pressure for T Mode at active state in the DEM simulation

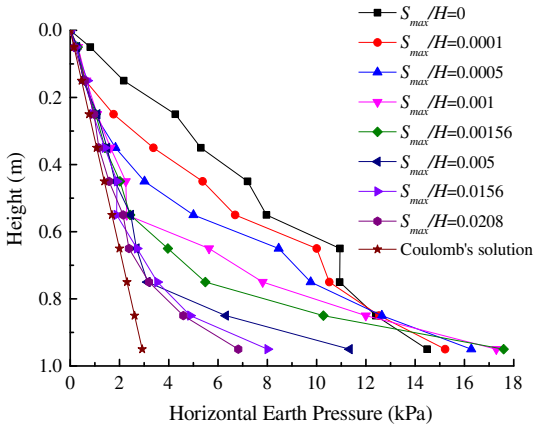

Fig. 11 Distribution of Horizontal Earth Pressure for RB Mode at active state in the DEM simulation

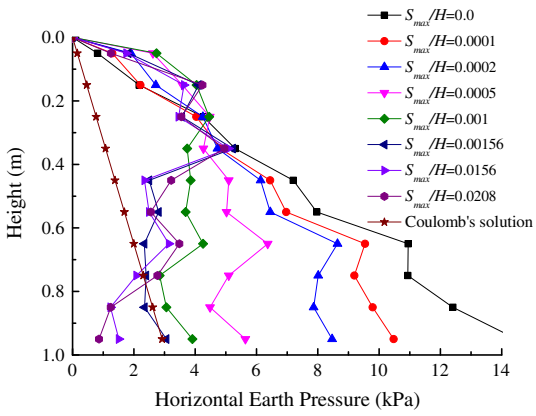

Fig. 12 Distribution of Horizontal Earth Pressure for RT Mode at active state in the DEM simulation

To gain more insights into the earth pressure mobilized, we examine the shear strain fields of the granular backfill in the three displacement modes as shown in Fig. 13. The

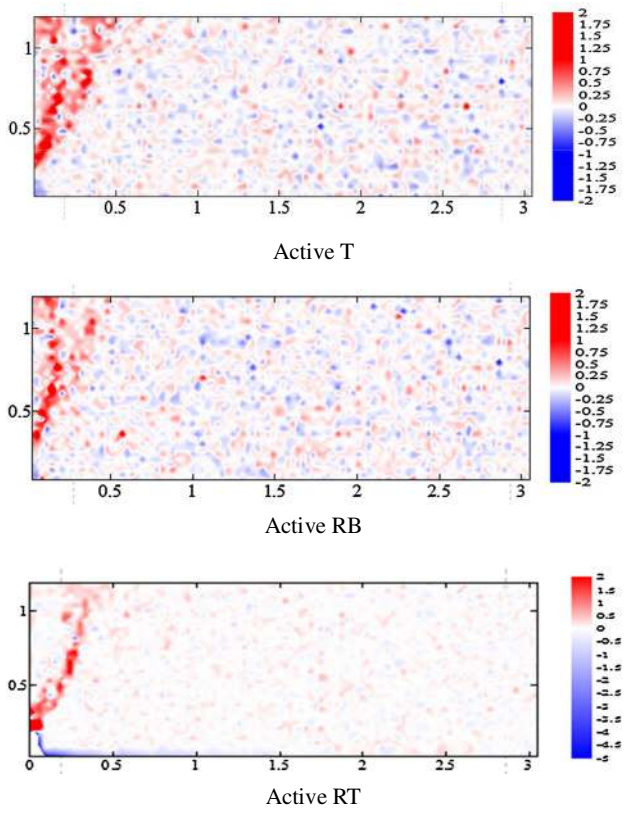

Fig. 13 Shear strain field in the medium-dense backfill at active mode in the case of $S_{max}/H = 0.0156$ obtained from the DEM simulations

shear strain fields are generated using the mesh-free method proposed by Wang and Gutierrez [50] and Wang et al. [72]. It is found that at a displacement of $S_{max}/H = 0.0156$, a distinct inclined shear band has developed in RT mode, corresponding to the limit active earth pressure mobilized at this large deformation stage, while the strain is less localized in the other two modes. The inclination angle of the shear bands is in the range of 58°–64°, and the thickness of the shear bands is about 9.52–21.8 mm, i.e., (7–16) d_{50}.

6 Passive earth pressure under different displacement modes

Figure 14 provides the passive total earth pressure and its point of the resultant with the changing displacement in the three modes. In contrast to the active case, the total thrust now increases rapidly and reaches a relatively stable value at large displacement in the T mode and RT mode. Such a trend is less well-defined in the RB mode, lacking of a clear stable regime within the applied displacement range. Similar to the active case, a larger deviator stress is mobilized in the T mode, resulting in a larger total passive thrust than in the other two modes. The location of the resultant in the T mode is nearly equal to 0.33, but slightly above and below 0.33 in

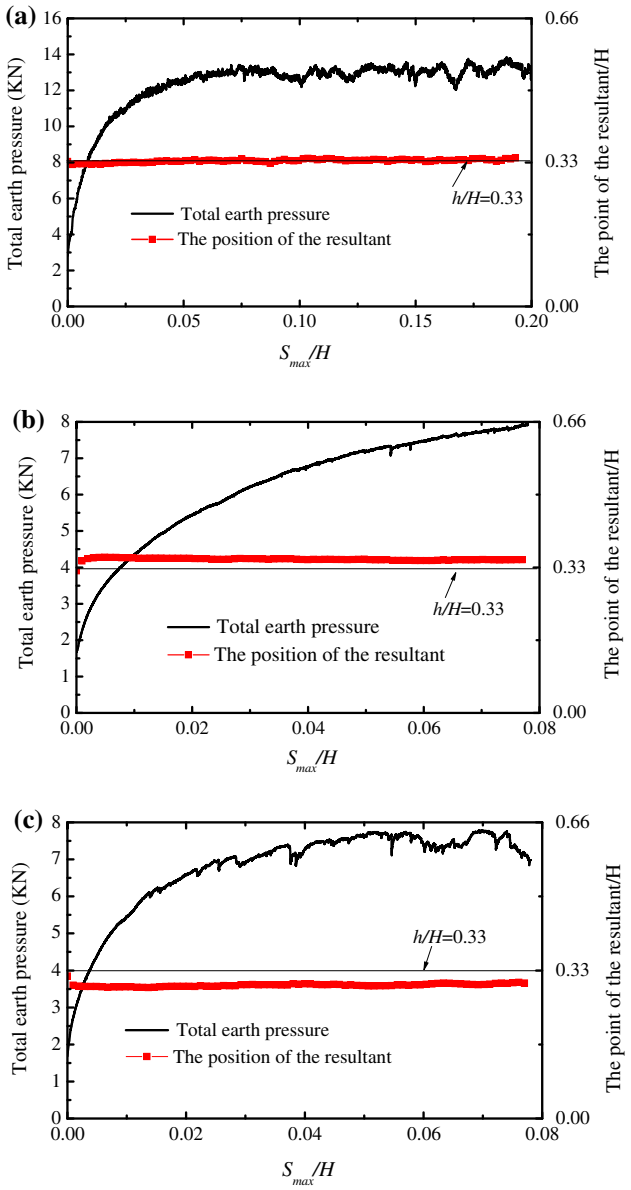

Fig. 14 Total earth pressure against the retaining wall and the point of the resultant with changing displacement at passive state: **a** T mode; **b** RB mode; **c** RT mode

the RB mode and RT mode, respectively. The latter result is opposite to that of the active case, resulting from the different earth pressure distributions in the passive case.

Figure 15 shows the normalized resultant passive earth pressure coefficient K_h obtained in the passive case. The values of K_h in each displacement mode increases and gradually reach a stable value. The value of K_h of T mode obtained from the simulations is reasonable in terms of the order of magnitude compared with the theoretical value according to Coulomb's solution (i.e., $K_h = 7.96$). Detailed distributions of earth pressure along the height of the wall in the three modes are shown in Figs. 16, 17, and 18, in which the the-

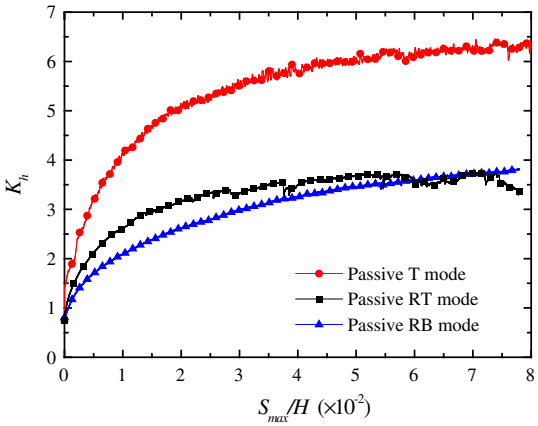

Fig. 15 The normalized resultant passive earth pressure coefficient K_h with changing displacement in T mode, RB mode and RT mode at passive state obtained from the DEM simulation

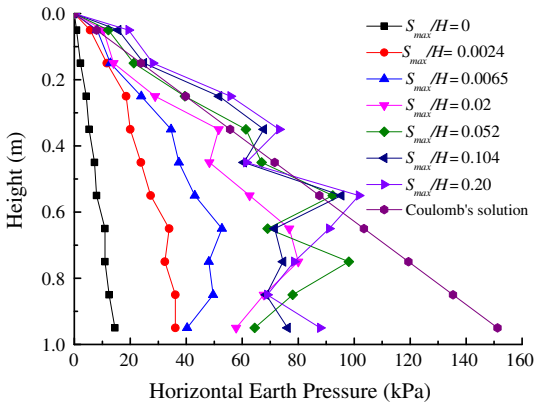

Fig. 16 Distribution of Horizontal Earth Pressure for T Mode at passive state in the DEM simulation

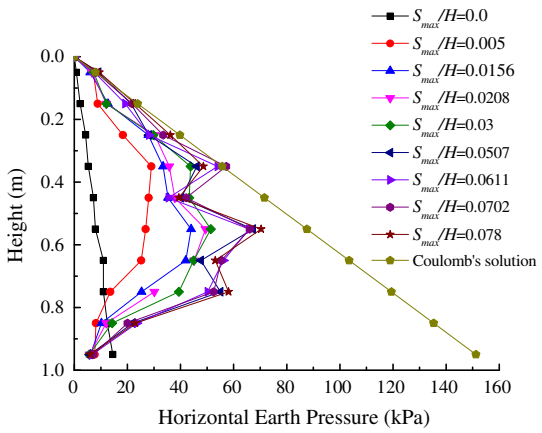

Fig. 17 Distribution of Horizontal Earth Pressure for RB Mode at passive state in the DEM simulation

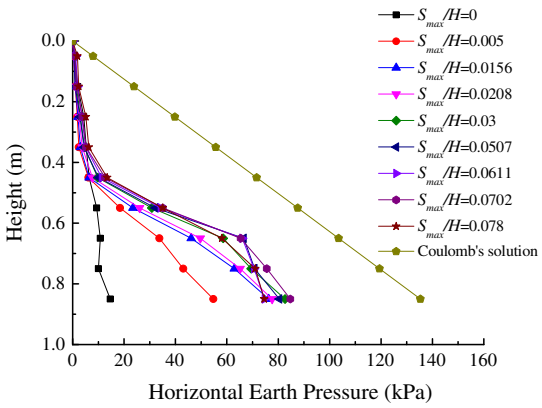

Fig. 18 Distribution of Horizontal Earth Pressure for RT Mode at passive state in the DEM simulation

oretical asymptote according to Coulomb's theory with the related value of the friction angle was added to facilitate a comparison to the analytical results. Increasing earth pressures with the wall displacement are found in each mode, with the limit passive earth pressure reached at a larger displacement in the T mode than in the other two modes. The degrees of nonlinearity of the earth pressure profiles are generally higher than those of the active case, which is resulted from the higher degrees of the non-uniformity of strain localization.

The shear strain fields shown in Fig. 19 illustrate the shear bands developed at large displacement in the three modes. Compared with the results obtained in the active mode (see Fig. 13), the passive wall motions give rise to a larger inclination of the shear bands, indicating the involvement of a larger amount of matrix soil in the strain localization process. Note that not all contacts in the shear band arrive at a plastic stage at large displacement in the three modes. For example, the percentage of contacts within the shear band in Passive T mode arriving at a plastic state in the tangential direction (i.e. sliding) and in the rotation direction is 57.9 % and 34.8 %, respectively, at $S_{max}/H = 0.15$ in Fig. 19. Besides, only a low percentage of contacts in the ground arrive at a plastic stage at large displacement in the three modes, e.g., 3.83 % and 2.13 % in the tangential direction and in the rotation direction, respectively, at $S_{max}/H = 0.15$ in Passive T mode, which indicates that the boundary effect must be quite little.

In the case of passive RB, the pattern of strain localization is a triangle form behind the retaining wall. The pattern of strain localization of passive RT is similar to that of passive T mode, while the strain localization in the case of T mode is much obvious. The inclination of the shear bands obtained in the simulations is in the range of 24°–30°, and the thickness is about 11 mm (i.e., $8d_{50}$).

7 Discussions

7.1 Effect of the initial density of the backfill

The effect of the initial density of the backfill was investigated through DEM simulations of the wall subjected to passive

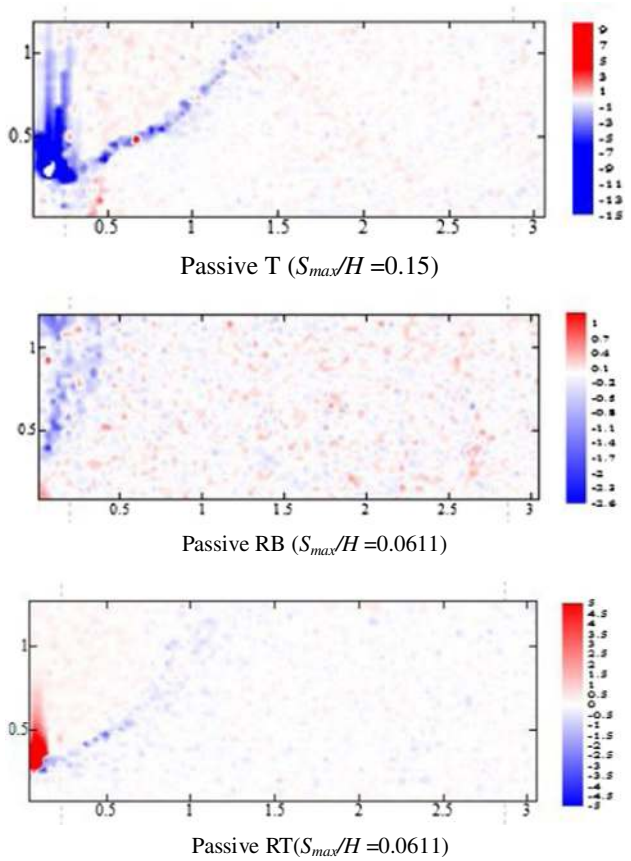

Fig. 19 Shear strain field in the medium-dense backfill at passive mode obtained from the DEM simulations

displacements and embedded in backfills with different initial void ratios, i.e., $e = 0.20$ (denoted as dense), 0.22 (denoted as medium A), 0.25 (denoted as medium B), and 0.33 (denoted as loose), while the other parameters remained the same.

Figure 20 presents the simulation results obtained from the biaxial compression tests under a confining pressure of 25 kPa on samples of different void ratios. It is clear that the typical deviatoric stress-volumetric strain-axial strain relationships of a dense sand were obtained at $e = 0.20$. The features of dilatancy-induced strength and subsequent strain-softening are much less pronounced in the two medium-dense samples than the dense one. In contrast, the sample with $e = 0.33$ exhibits strain-hardening and volumetric contractive behavior as a typical loose granular material. Nevertheless, the stress-strain relationships of all samples coincide at large axial strains once the critical state is approached, indicating that the residual strength remains approximately the same regardless of the initial density of the samples. The biaxial compression simulations were also performed under other confining pressures (i.e., 100 and 200 kPa), and the corresponding results are tabulated in Table 3, which confirms that the samples of different initial density have different values of the peak internal friction angle but have almost an identical value of the residual friction angle about 23°.

Table 3 Strength indexes of the backfill samples at different initial void ratios

Sample no.	Void ratio e	Description	Peak internal friction angle	Residual internal angle
1	0.20	Dense	35.2°	23.5°
2	0.22	Medium dense A	32.4°	23.1°
3	0.25	Medium dense B	29.3°	22.6°
4	0.33	Loose	22.6°	22.6°

Figure 21 provides the normalized resultant earth pressure coefficient K_h of backfills with different initial densities when the wall is subjected to passive T mode movement. As shown in Fig. 21a, the simulated K_h—displacement diagram is strongly affected by the void ratio of the backfill. The coefficient K_h monotonically increases against the displacement (i.e., 'hardening') in the case of a loose backfill at $e = 0.33$. With the decrease of the void ratio, K_h gradually exhibits

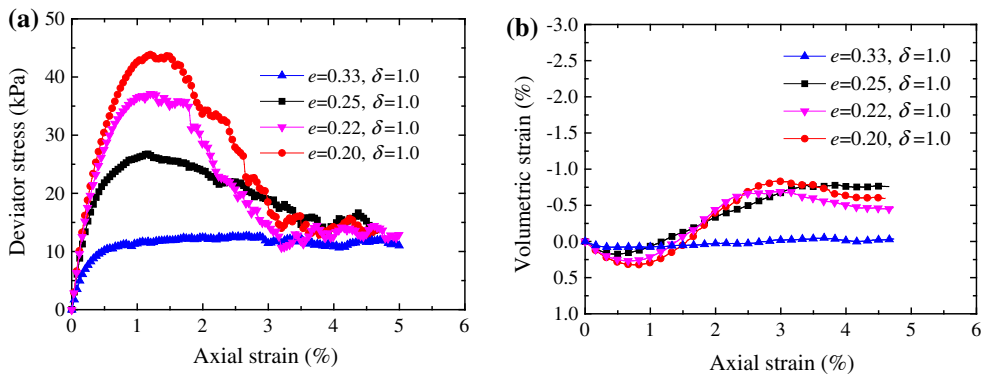

Fig. 20 Mechanical behavior obtained from the DEM biaxial compression tests on the sample with four different void ratios: **a** stress–strain behavior; **b** volumetric strain response

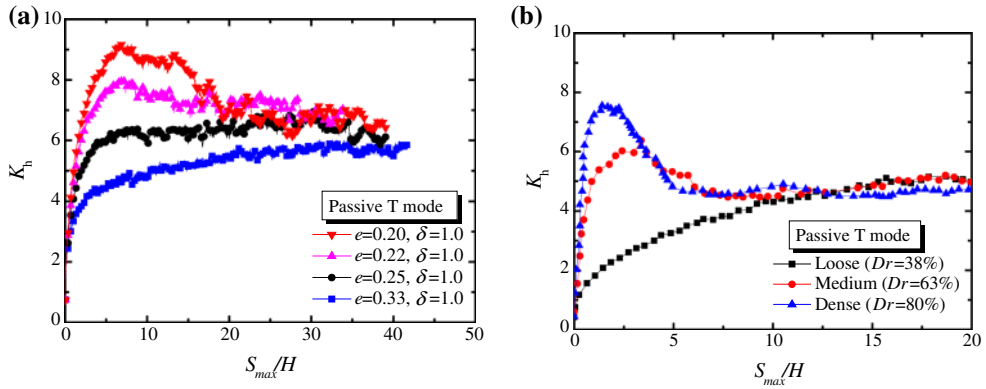

Fig. 21 The normalized resultant passive earth pressure coefficient K_h obtained from backfills with different void ratios: **a** DEM simulation; **b** experiments conducted by Fang et al. [16]

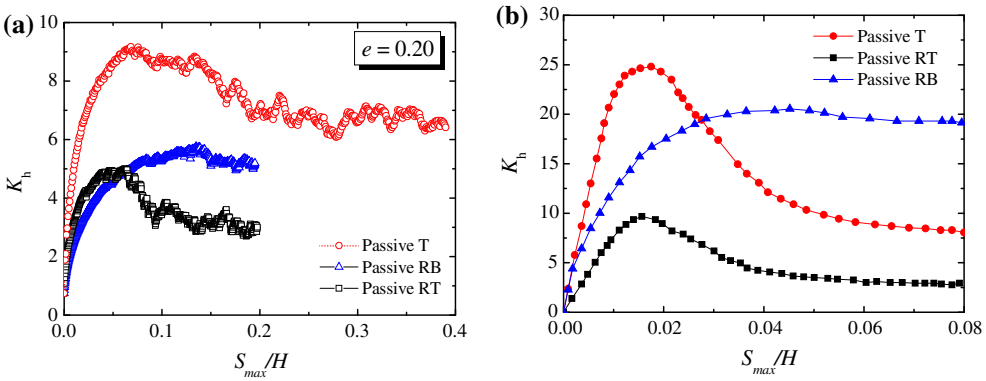

Fig. 22 The normalized resultant passive earth pressure coefficient K_h for an initially dense material: **a** DEM simulation in this study; **b** DEM simulation conducted by Widulinski et al. [35]

'softening'. This agrees well with the experimental observation under different relative densities [16] as illustrated in Fig. 21b. It is noted that strain-softening response in the element tests does not necessarily result in softening response in K_h—displacement diagram. For instance, K_h is softening at $e = 0.22$ and hardening at $e = 0.25$, although both cases exhibit softening in the biaxial compression test simulations as shown in Fig. 20a.

Figure 22a presents the normalized resultant passive earth pressure coefficient K_h obtained from the dense case (i.e., $e = 0.20$) when the wall is subjected to different passive displacement modes. In contrast to Fig. 15a in the medium-dense case, Fig. 22a shows that K_h increases up to the peak and then decreases to a steady value in the cases of T mode and RT mode, while it continuously increases up to a steady value in the case of RB mode. Compared to the DEM results obtained by Widulinski et al. [35] shown in Fig. 22b, our DEM results show that the variation of the normalized resultant passive earth pressure coefficient K_h for an initially dense material agrees qualitatively with the results obtained by Widulinski et al. [35], although there exists some quantitative differences between them. Such quantitative differences come from the fact that different internal friction angle and different coefficient of wall friction are used in the two cases. Figure 23 presents the shear strain field obtained from DEM simulations in comparison with the experimental results [64]. Similar to experimental results, DEM simulations show that the strain localization is more obvious in T mode and RT mode than RB mode.

Figure 24a provides the normalized resultant passive earth pressure coefficient K_h obtained from the loose case (i.e., $e = 0.33$) when the wall is subjected to different passive displacement modes. Different from Fig. 22a, K_h in Fig. 24a presents hardening behavior regardless of the displacement modes. This agrees well with the experimental observation made by Fang et al. [18] using an initially loose sand with relative density $Dr = 19.2\,\%$ as show in Fig. 24b. Figure 25 presents the shear strain field obtained from DEM simulations in the loose case in comparison with the experimental results obtained by Niedostatkiewicz et al. [71] under similar conditions. Similar to the dense case (see Fig. 23), simulations and experiments in the loose case both show that the strain localization is less obvious in the RB mode than that in the other two modes.

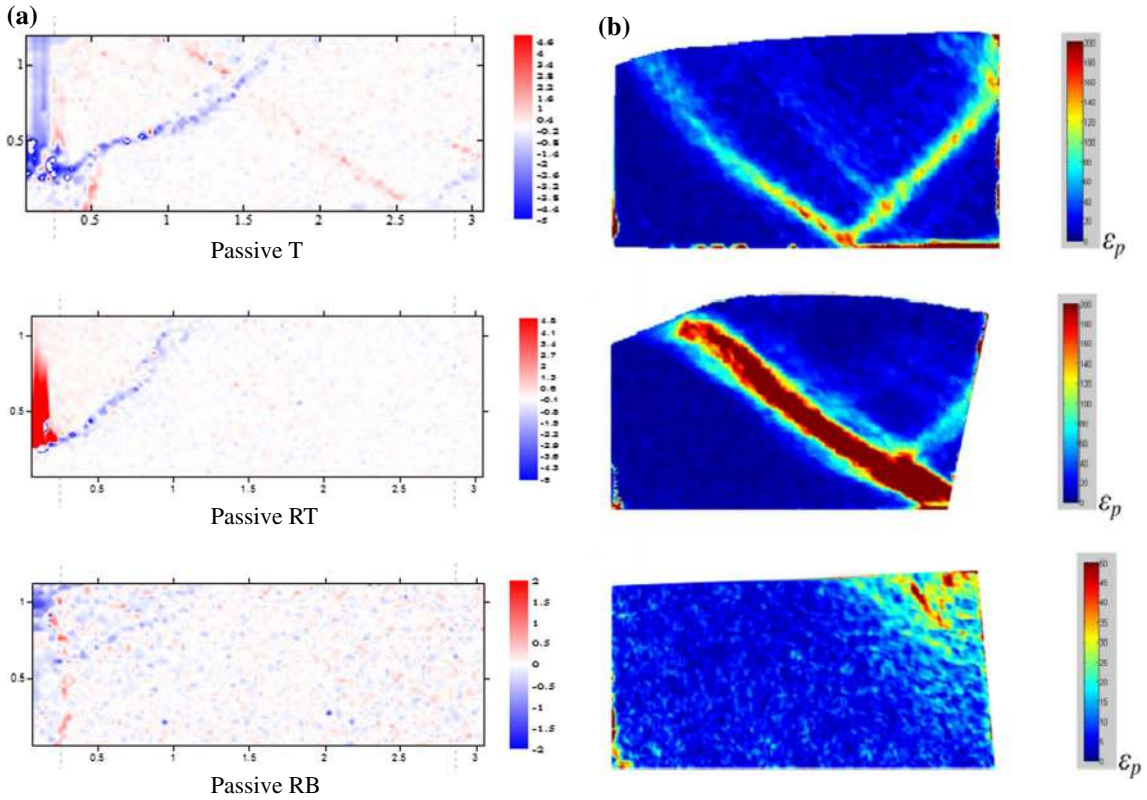

Fig. 23 Shear strain field in initially dense backfill obtained from: **a** DEM simulations; **b** DIC experiments conducted by Niedostatkiewicz et al. [71]

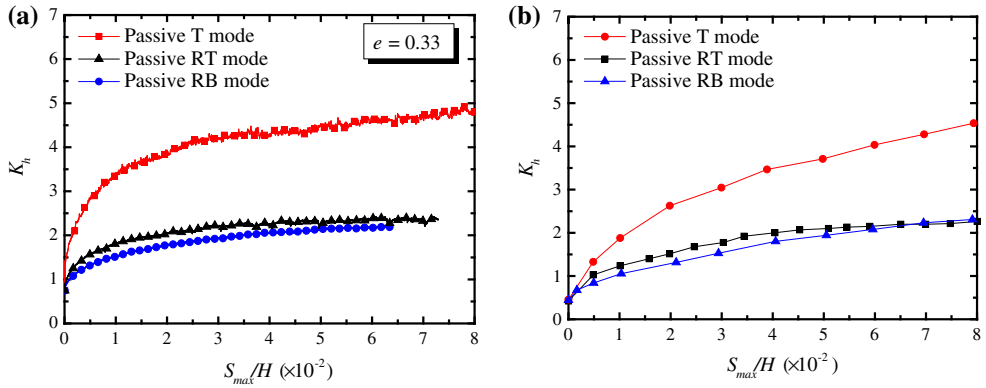

Fig. 24 The normalized resultant passive earth pressure coefficient K_h for an initially loose material: **a** DEM simulation; **b** experiments conducted by Fang et al. [18]

7.2 Effect of the mean grain size

The effect of the mean grain diameter, d_{50}, was investigated by changing the size of soil particles used in the DEM simulations while the other parameters including the initial density of backfills remained unchanged. Three configurations of the particle gradation were used: (1) the small case with a particle size range of 0.78–1.94 mm with $d_{50} = 1.36$ mm; (2) the medium case with a particle size range of 1.014–2.522 mm with $d_{50} = 1.768$ mm; and (3) the large case with a particle size range of 1.56–3.88 mm with $d_{50} = 2.72$ mm. Note that the gradation curves of these three cases are parallel.

Figure 26 presents the effect of the mean grain diameter on the coefficient K_h when the wall is subjected to a passive translational movement. Despite of the initial density of backfills, the coefficient K_h increases with the increase of the mean grain size. However, the difference between the medium case and the large case is less appreciable.

Note that, in this paper, we used two-dimensional DEM to study earth pressure against a rigid retaining wall under vari-

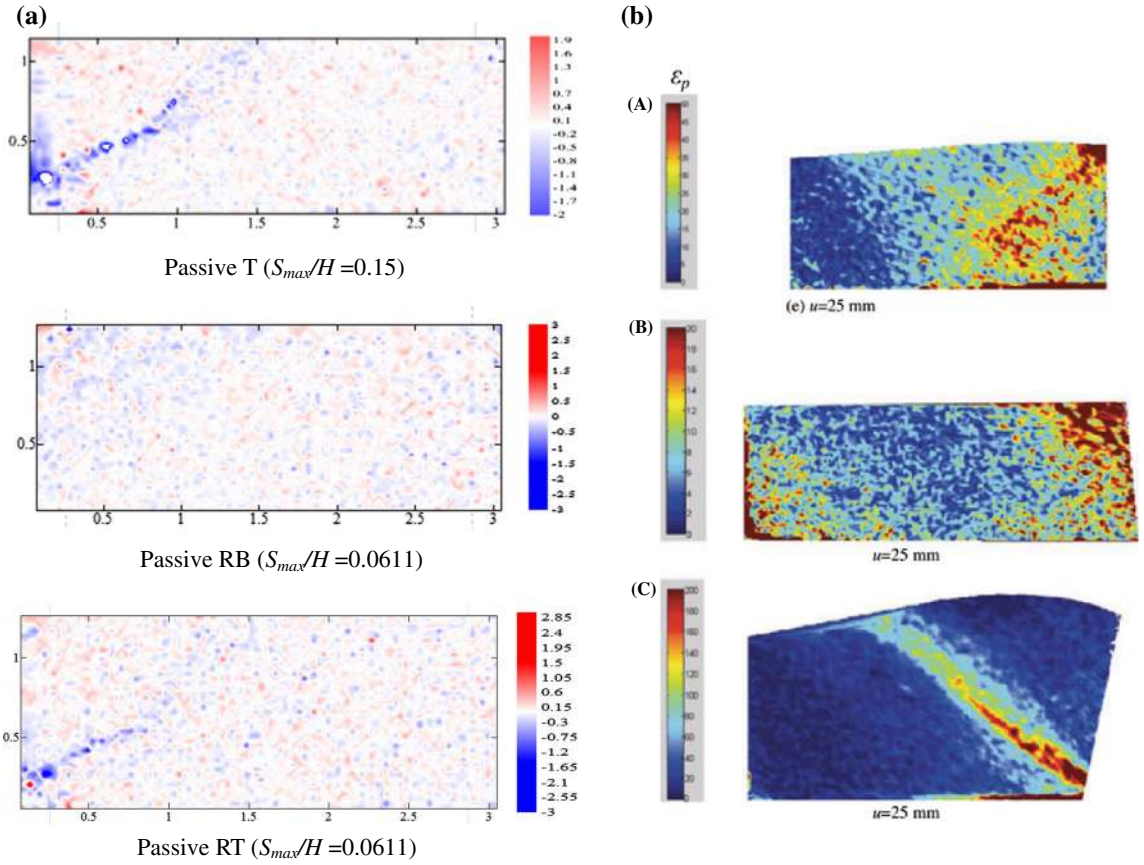

Fig. 25 Shear strain field in initially loose backfill obtained from: **a** DEM simulations; **b** DIC experiments conducted by Niedostatkiewicz et al. [71]

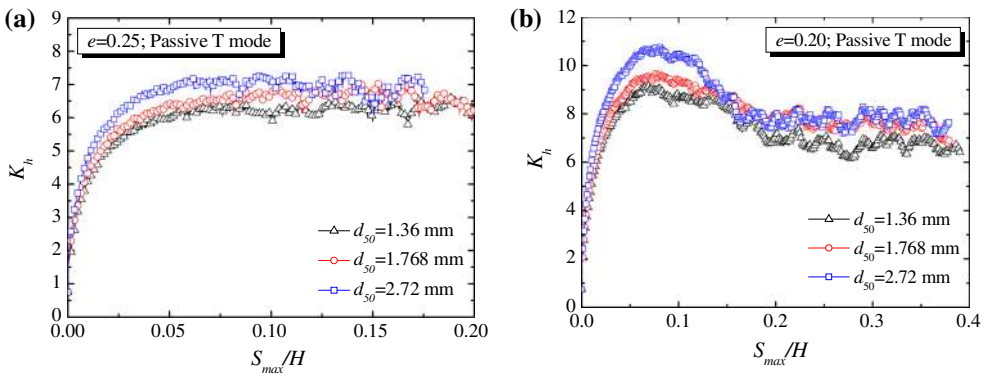

Fig. 26 Effect of the mean grain size on the earth pressure coefficient: **a** medium dense backfill; **b** dense backfill

ous wall movement modes with a contact model considering different inter-particle rolling resistances. The substantive characteristics of choosing different rolling resistance coefficients under the same void ratio are to change the relative density of the specimen (Dr). A realistic value of the internal friction angle of soils can be produced by using the rolling resistance contact model with a properly selected value of δ, due to the peak and residual friction angles increase with the increasing of rolling resistance coefficient given the same void ratio.

We did not aim to simulate a realistic granular material completely (e.g., Ottawa silica sand) with a 2D DEM. This is because 2D DEM is not good enough to capture the post-failure volumetric strain behavior of materials since the particles cannot move spatially into adjacent voids as accurately as in three-dimensional simulations. Although three-

dimensional (3D) DEM appears to be a promising option for the analyses, the 2D modeling is the only possible choice at this stage. This is because the size effect and boundary effect must be reduced to the minimum in the DEM analysis of the large-scale boundary-value problem in the study, which requires an extremely large number of particles and which analysis is possible only by 2D DEM for current PCs. In addition, in terms of visualizing stress fields and velocity fields etc., 2D DEM is better than 3D DEM. Besides, from the geotechnical engineering viewpoint, 2D DEM can capture the strength features of soils, with reasonable contact models and carefully determined parameters, as well as the material failure and instability, which is the most important for the boundary-value problem in the study.

8 Conclusion

The paper considers the influence of inter-particle rolling resistance in the sandy backfill for the active and passive earth pressure of a translating retaining wall. The earth pressure against a rigid retaining wall under various wall movement modes is analyzed with a contact model considering inter-particle rolling resistance implemented into the DEM. Earth pressure law is examined from the microscopic particle scale as well as the macroscopic scale. The DEM simulation outcomes considering inter-particle rolling resistance are appropriate and are in line with the previous experimental results.

(1) Considering inter-particle rolling resistance, the amount and the position of the earth pressure are distinct in different displacement modes of the retaining wall. The more displacement quantities the wall moves toward the soil mass, the greater the resultant force is; the greater displacement quantities the wall moves away the soil mass, the smaller the total earth pressure is. The point of the resultant slightly differs from the position of Coulomb theory $0.33H$, and it varies with displacement modes.
(2) The evolution of the normalized resultant earth pressure coefficient K_h is affected by the wall displacement modes. In the case of medium dense backfills $e = 0.25$, the coefficient K_h drops rapidly at the beginning and then reaches a constant with increasing wall displacement in the active state, while it rapidly increases and then gradually approaches a constant in the passive state.
(3) The normalized resultant earth pressure coefficient K_h is strongly affected by the initial density of backfills. When the wall is subjected to translational passive movement, the K_h changes nonlinearly with the increase of wall displacement, switching from the hardening to the softening as the initial state of the packed backfills changes from the loose to the dense. In contrast, the $K_h - S_{max}/H$ relation demonstrates either hardening or softening feature for the medium-dense backfills even they exhibit a strain-softening response in the biaxial compression tests.
(4) The earth pressure coefficient K_h increases with increasing particle size in the small strain, while the distinct difference begins to become inconspicuous among the three cases of mean grain size when the critical state is reached.

Acknowledgments The research was funded by the China National Funds for Distinguished Youth Scientists with Grant No. 51025932, the National Natural Science Foundation of China with Grant Nos. 41102173, 51109182. All the supports are greatly appreciated. The authors would also like to thank the comments from two anonymous reviewers that certainly improved the quality of the paper.

References

1. Coulomb C.A.: Essai sur une application des regles des maximis et minimis a quelques problemes de statique relatifs a l'architecture. Memoires de l'Academie Royale pres Divers Savants, vol. 7, pp. 343–387 (in French)
2. Rankine, W.J.M.: On the stability of loose earth. Scotl. Philos. Trans. R. Soc. Lond. **147**, 9–27 (1857)
3. Bang, S.: Active earth pressure behind retaining walls. J. Geotech. Eng. (ASCE) **111**(3), 407–412 (1985)
4. Handy, R.L.: The arch in soil arching. J. Geotech. Eng. (ASCE) **111**(3), 302–318 (1985)
5. Harrop-Williams, K.: Arching in soil arch. J. Geotech. Eng. (ASCE) **115**(3), 415–419 (1989)
6. Paik, K.H., Salgado, R.: Estimation of active earth pressure against rigid retaining walls considering arching effect. Geotechnique **53**(7), 643–645 (2003)
7. Chang, M.F.: Lateral earth pressure behind rotating walls. Can. Geotech. J. **34**(2), 498–509 (1997)
8. Terzaghi, K.: Record earth pressure testing machine. ENR **109**(29), 365–369 (1932)
9. Terzaghi, K.: Large retaining wall test I-pressure of dry sand. ENR **112**(1), 136–140 (1934)
10. Terzaghi, K.: Large retaining wall test II-pressure of saturated sand. ENR **112**(22), 259–262, 316–318, 403–406, 503–508 (1934)
11. Schofield, A.N.: The development of lateral force of sand against the vertical face of a rotating model foundation. In: Proceedings of the 5th International Conference on Soil Mechanics and Foundation Engineering, Paris, vol. 2, pp. 479–494 (1961)
12. Matteotti, G.: Some results of quay-wall model tests on earth pressure. Proc. Inst. Civ. Eng. Lond. **47**, 184–204 (1970)
13. Bros, B.: The influence of model retaining wall displacements on active and passive earth pressure in sand. In: Proceedings of the 5th European Conference on Soil Mechanics, vol. 1, pp. 241–249 (1972)
14. Sherif, M.M., Mackey, R.D.: Pressure on retaining wall with repeated loading. J. Geotech. Eng. (ASCE) **103**(11), 1341–1345 (1977)
15. Matsuo, M., Kenmochi, S., Yagi, H.: Experimental study on earth pressure of retaining wall by field test. Soils Found. **18**(3), 27–41 (1978)
16. Fang, Y.S., Ho, Y.C., Chen, T.J.: Passive earth pressure with critical state concept. J. Geotech. Eng. (ASCE) **128**(8), 651–659 (2002). http://ascelibrary.org/doi/abs/10.1061/%28ASCE%291090-0241%282002%29128%3A8%28651%29

17. Fang, Y.S., Ishibashi, I.: Static earth pressure with various wall movements. J. Geotech. Eng (ASCE) **112**(3), 317–333 (1986)
18. Fang, Y.S., Chen, T.J., Wu, B.F.: Passive earth pressure with various wall movements. J. Geotech. Eng. (ASCE) **120**(8), 1307–1323 (1994)
19. Clough, G.W., Duncan, J.M.: Finite element analysis of retaining wall behavior. J. Geotech. Eng. (ASCE) **97**(12), 1657–1673 (1971)
20. Ozawa, Y., Duncan, J.M.: Elasto-plastic finite element analyses of sand deformations. In: Proceedings of 2nd International Conference on Numerical Methods in Geomechanics, Blacksburg, USA, pp. 243–263 (1976)
21. Nakai, T.: Analysis of earth pressure problems considering the influence of wall friction and the wall deflection. In: Proceedings of the 5th International Conference on Numerical and Analytical Methods in Geomechanics. Nagoya, Japan, pp. 765–772 (1985)
22. Potts, D.M., Fourie, A.B.: A numerical study of the effects of wall deformation on earth pressure. Int. J. Numer. Anal. Methods Geomech. **10**, 383–405 (1986)
23. Bhatia, S.K., Bakeer, R.M.: Use of the finite element method in modeling a static earth pressure problem. Int. J. Numer. Anal. Methods Geomech. **13**, 207–213 (1989)
24. Matsuzawa, H., Hazarika, H.: Analyses of active earth pressure against rigid retaining walls subjected to different modes of movement. Soils Found. **36**(3), 51–65 (1996)
25. Rudnicki, J.W., Rice, J.R.: Conditions for the localization of deformation in pressure-sensitive dilatant materials. J. Mech. Phys. Solids **23**, 371–394 (1975)
26. Vardoulakis, I.: Shear band inclination and shear modulus of sand in biaxial tests. Int. J. Numer. Anal. Methods Geomech. **4**, 103–119 (1980)
27. Papamichos, E., Vardoulakis, I.: Shear band formation in sand according to non-coaxial plasticity model. Géotechnique **45**, 649–661 (1995)
28. Yatomi, C., Yashima, A., Iizuka, A., Sano, I.: General theory of shear bands formation by a noncoaxial Cam-clay model. Soils Found. **29**(3), 41–53 (1989)
29. Hazarika, H., Matsuzawa, H.: Wall displacement modes dependent active earth pressure analyses using smeared shear band method with two bands. Comput. Geotech. **19**, 193–219 (1996)
30. Jiang, M.J., Yan, H.B., Zhu, H.H., Utili, S.: Modeling Shear behavior and strain localization in cemented sands by two-dimensional distinct element method analyses. Comput. Geotech. **38**, 14–29 (2011)
31. Zienkiewicz, O.C., Taylor, R.L.: The Finite Element Method for Solid and Structural Mechanics. Butterworth-Heinemann, London (2005)
32. Nübel, K., Huang, W.X.: A study of localized deformation pattern in granular media. Comput. Methods Appl. Mech. Eng. **193**(27), 2719–2743 (2004)
33. Tejchman, J., Bauer, E., Tantono, S.F.: Influence of initial density of cohesionless soil on evolution of passive earth pressure. Acta Geotechnica. **2**(1), 53–63 (2007)
34. Tejchman, J., Wei, W.: Boundary effects on behaviour of granular material during plane strain compression. Eur. J. Mech. A Solids **29**(1), 18–27 (2010)
35. Widuliński, Ł., Tejchman, J., Kozicki, J., Leśniewska, D.: Discrete simulations of shear zone patterning in sand in earth pressure problems of a retaining wall. Int. J Solids Struct. **48**(7–8), 1191–1209 (2011)
36. Tejchman, J.: Influence of a characteristic length on shear zone formation in hypoplasticity with different enhancements. Comput. Geotech. **31**, 595–611 (2004)
37. Nitka, M., Tejchman, J.: A two-scale numerical approach to granular systems. Arch. Civ. Eng. **3**, 595–611 (2011)
38. Nitka, M., Combe, G., Dascalu, C., Desrues, J.: Two-scale modeling of granular materials: a DEM–FEM approach. Granul. Matter. **13**(3), 277–281 (2011)
39. Jiang, M.J., Yu, H.S., Harris, D.: Kinematic variables bridging discrete and continuum granular mechanics. Mech. Res. Commun. **33**, 651–666 (2006)
40. Jiang, M.J., Leroueil, S., Zhu, H.H., Yu, H.S., Konrad, J.M.: Two-dimensional discrete element theory for rough particles. Int. J. Geomech (ASCE) **9**(1), 20–33 (2009)
41. Jiang, M.J., Zhu, H.H.: An interpretation of the internal length in Chang's couple-stress continuum for bonded granulates. Granul. Matter **9**, 431–437 (2007)
42. Jiang, M.J., Harris, D., Zhu, H.H.: Future continuum models for granular materials in penetration analyses. Granul. Matter **9**, 97–108 (2007)
43. Cundall, P.A., Strack, O.D.L.: The discrete numerical model for granular assemblies. Géotechnique **29**(1), 47–65 (1979)
44. Cundall, P.A., Strack, O.D.L.: The Distinct Element Method as a Tool for Research in Granular Media. Part II. Department of Civil Engineering Report, University of Minnesota, Minnesota (1979)
45. Cundall, P.A.: Discontinuous future for numerical modeling in geomechanics. Geotech. Eng. **149**(1), 41–47 (2001)
46. Itasca Consulting Group Inc.: Particle Flow Code in 2 Dimensions, PFC2D Version 3.0. Minneapolis (2002)
47. Jiang, M.J., Leroueil, S., Konrad, J.M.: Insight into shear strength functions of unsaturated granulates by DEM analyses. Comput. Geotech. **31**, 473–489 (2004)
48. Thornton, C.: Numerical simulation of deviatoric shear deformation of granular media. Géotechnique **50**, 43–53 (2000)
49. Jiang, M.J., Yu, H.S., Harris, D.: Bond rolling resistance and its effect on yielding of bonded granulates by DEM analyses. Int. J. Numer. Anal. Methods Geomech. **30**, 723–761 (2006)
50. Wang, J., Gutierrez, M.S.: Discrete element simulation of direct shear specimen scale effects. Géotechnique **60**(5), 395–409 (2010)
51. Pohl, M., Pulsfort, M., Walz, B.: Application of PFC3D for determination of soil properties and simulation of the excavation process in front of sheet pile wall constructions. In: Shimizu, Y., Hart, R., Cundall, P.A. (eds.) Numerical Modeling in Micromechanics Via Particle Methods, pp. 35–44. Taylor & Francis Group, London (2004)
52. Jiang, M.J., Yu, H.S., Harris, D.: Discrete element modelling of deep penetration in granular soils. Int. J Numer. Anal. Methods Geomech. **30**, 335–361 (2006)
53. Jenck, O., Dias, D., Kastner, R.O.: Discrete element modelling of a granular platform supported by piles in soft soil—validation on a small scale model test and comparison to a numerical analysis in a continuum. Comput. Geotech. **36**, 917–927 (2009)
54. Jiang, M.J., Shen, Z.F., Zhu, F.Y.: Numerical analyses of braced excavation in granular grounds: continuum and discrete element approaches. Granul. Matter **15**(2), 195–208 (2013)
55. Chang, C.S., Chao, S.J.: Discrete element analysis for active and passive pressure distribution on retaining wall. Comput. Geotech. **16**(4), 291–310 (1994)
56. Mirghasemi, A.A., Javan, M.R.M.: Discrete element method analysis of retaining wall earth pressure in static and pseudo-static conditions. Iran. J. Sci. Technol. **30**(B1), 145–150 (2006)
57. Zhao, T., Jiang, M.J.: DEM analysis of an inclining rigid retaining wall subjected to translation movement mode. In: International Symposium on Geomechanics and Geotechnics: From Micro to Macro, vol. 2, pp. 543–549 (2010)
58. Kress, J.G.: An investigation into Soil-Structure Interaction Problems using Discrete Element Method. M.A. thesis, North Carolina State University, USA (2011)
59. Oda, M., Konishi, J., Nemat-Nasser, S.: Experimental micromechanical evaluation of strength of granular materials: effects of particle rolling. Mech. Mater. **1**, 269–283 (1982)

60. Oda, M., Kazama, H.: Micro-structure of shear band and its relation to the mechanism of dilatancy and failure of granular soils. Géotechnique **48**, 465–481 (1998)
61. Iwashita, K., Oda, M.: Rolling resistance at contacts in simulation of shear band development by DEM. J. Eng. Mech. **124**(3), 285–292 (1998)
62. Iwashita, K., Oda, M.: Micro-deformation mechanism of shear banding process based on modified distinct element. Powder Technol. **109**(1–3), 192–205 (2000)
63. Mohamed, A., Gutierrez, M.: Comprehensive study of the effects of rolling resistance on the stress-strain and strain localization behavior of granular materials. Granul. Matter **12**(5), 527–541 (2010)
64. Chang, C.S., Liao, C.L.: Constitutive relation for a particulate medium with effect of particle rotation. Int. J. Solids Struct. **26**, 437–453 (1990)
65. Chang, C.S., Ma, L.A.: Micromechanical-based micropolar theory for deformation of granular solids. Int. J Solids Struct. **28**, 67–86 (1991)
66. Chang, C.S., Gao, J.: Second-gradient constitutive theory for granular material with random packing structure. Int. J Solids Struct. **32**, 2279–2293 (1995)
67. Zhou, Y.C., Wright, B.D., Yang, R.Y., Xu, B.H., Yu, A.B.: Rolling friction in the dynamic simulation of sandpile formation. Phys. A Stat. Mech. Appl. **269**, 536–553 (1999)
68. Sakaguchi, H., Ozaki, E., Igarashi, T.: Plugging of the flow of granular materials during the discharge from a silo. Int. J. Mod. Phys. B **7**, 1949–1949 (1993)
69. Jiang, M.J., Yu, H.S., Harris, D.: A novel discrete model granular material incorporating rolling resistance. Comput. Geotech. **32**(5), 340–357 (2005)
70. Jiang, M.J., Konrad, J.M., Leroueil, S.: An efficient technique for generating homogeneous specimens for DEM studies. Comput. Geotech. **30**(7), 579–597 (2003)
71. Niedostatkiewicz, M., Lesniewska, D., Tejchman, J.: Experimental analysis of shear zone patterns in cohesionless for earth pressure problems using particle image velocimetry. Strain **47**(s2), 218–231 (2011)
72. Wang, J., Gutierrez, M.S., Dove, J.E.: Numerical studies of shear banding in interface shear tests using a new strain calculation method. Int. J Numer. Anal. Methods Geomech. **31**(12), 1349–1366 (2007)